

A model based on the equations of the gentle slope for wave propagation and sediment transport

Un modelo basado en las ecuaciones de pendiente suave para la propagación del oleaje y el transporte de sedimentos

DOI: 10.26640/22159045.430

Reception date: 2017-05-18 / Acceptance date: 2017-08-14

Isabel María Ramos de la Hoz*, Álvaro Galán, Serguei Lonin*** & Alejandro Orfila.******

Ramos de la Hoz, I., Galán, A., Lonin, S. & Orfila, A. (2017). *A model based on the equations of the gentle slope for wave propagation and sediment transport.* Bol. Cient. CIOH (35):25-40. ISSN 0120-0542 e ISSN en línea 2215-9045. DOI: 10.26640/22159045.430

ABSTRACT

The description of a phase model which solves the equations of wave propagation through the approximation of the mild slope is presented. The model, developed in the context of the "Litoral Project Model of the Coastal Zones - LIZC", performs a data processing that allows the transformation of a completely linear waves (no sediment transport) to a nonlinear wave in order to model sediment transport in shallow areas properly. In the simulation all possible sea states of a particular period are used, bearing in mind not only the influence of waves on the bottom, but also the effect of bottom on the waves; obtaining the evolution of the bathymetry for the period under study.

KEY WORDS: Numeric model, wave, mild slope equations, sediment transport, Galerazamba, LIZC

RESUMEN

Se presenta la descripción de un modelo de fase que resuelve las ecuaciones de propagación del oleaje mediante la aproximación de la pendiente suave ("Mild Slope"). El modelo, desarrollado dentro del marco del proyecto del modelo Litodinámico de la Zona Costera - LIZC, realiza un tratamiento de los datos que permite la transformación de un oleaje completamente lineal (sin transporte de sedimentos) en un oleaje no lineal, permitiendo así la modelación del transporte de sedimentos en la zona más somera. En la simulación se utilizan todos los posibles estados de mar de una determinada época, teniendo en cuenta no solo la influencia del oleaje sobre el fondo, sino también el efecto del fondo sobre el oleaje; permitiendo así obtener la evolución de la batimetría para la época en estudio.

PALABRAS CLAVE: modelo numérico, oleaje, ecuaciones de la pendiente suave, transporte de sedimentos, Galerazamba, LIZC.

* Oceanographic and Hydrographic Research Center - CIOH, Cartagena; Universidad del Norte, Barranquilla. E-mail: isaramos1014@gmail.com

** E.T.S.I. de Caminos, Canales y Puertos, UCLM, Ciudad Real, España. E-mail: Alvaro.Galan@uclm.es

*** Oceanographic and Hydrographic Research Center - CIOH, Naval Cadets Academy Almirante Padilla, Cartagena. E-mail: slonin@costa.net.co

**** IIMEDEA (CSIC-UIB), Esporles, Islas Baleares (España). E-mail: aorfila@imedea.uib-csic.es

INTRODUCTION

The numerical models of wave propagation try to simulate several mechanisms involved in the transformation of the waves. In coastal areas the dominant mechanisms are wave shoaling, refraction, and diffraction due to changes in the bathymetry or due to structures, reflection in the coastline, structures and changes in bathymetry, dissipation of energy due to breakage of the waves or friction with the seabed, interaction wave-current and wave-wave interaction. Except on extraordinary occasions, for very simple cases, it is not known in advance which of these phenomena are dominant for the objective pursued. The numerical models seek, in a computationally efficient way, to represent reality as efficiently and accurately as possible.

In general, mathematical models of wave propagation can be separated into two types: i) conservation models of mechanical energy and ii) conservation models of mass or momentum. Both types can incorporate, in a more or less appropriate manner, most of the mechanisms described above. However, energy models cannot capture the effects of diffraction and reflection caused by the variation of the seabed, and coastal structures. In contrast, conservation models of the mass or momentum are unable to incorporate wave-wave interaction induced by the wind and, in addition, are computationally more expensive. The research presented focused on the propagation equation for mild slope.

The equation for mild slope, hereafter MSE ("Mild Slope Equation"), is an effective conservation model of mass when simulating the wave shoaling produced in a coastal area in combination with refraction, reflection and diffraction, so it has become one of the most used equations since it was introduced by Berkhoff (1972). The model was decoupled by Copeland (1985), in a pair of equations in partial derivatives of the first order, obtaining the hyperbolic model and reducing

the computational costs of solving the initial elliptical model. Since then, there have been many researchers who have demonstrated the ability of hyperbolic MSE to describe the waves in the coastal zone (Song, Zhang, Kong, Li, and Zhang, 2007; Suh, Lee, and Park, 1997; Bokaris and Anastasiou, 2003; Lee, Park, Cho & Suh, 1998).

To solve numerically the proposed equations, implicit methods are generally used for temporal integration. Even so, numerical instabilities can appear, so it is usual to use artificial filters capable of absorbing these instabilities. However, the use of numerical filters causes a damping of the solution, which may alter the accuracy of this solution. Following the work of Galán, Simarro, G., Orfila, Simarro, J. & Liu (2012), this research has opted to use an explicit numerical scheme Runge-Kutta of 4th order for the temporal evolution, using an approximation for spatial derivatives up to order $O(\Delta x^2)$, where Δx as the mesh size.

STUDY AREA

Two different scenarios were used to analyze the performance of the model. The first makes use of the bathymetry of the experiment by Galan *et al.*, (2012), and is described later. For the second study scenario, the bathymetry of the Galerazamba-Colombia sector, provided by the Caribbean Oceanographic and Hydrographic Research Center-CIOH, was used. This zone is a sector without anthropic influence in the local scale, with a coastal spike that interacts with the terrestrial fluvial regime of the Ciénaga El Totumo and with the wave regime; presenting a strong diffraction at the tip of Galerazamba (Figure 1).

METHODOLOGY

This section contains the formulations of the model for the hydrodynamic and sediment transport modules, as well as some numerical experiments for the verification of the model's performance.

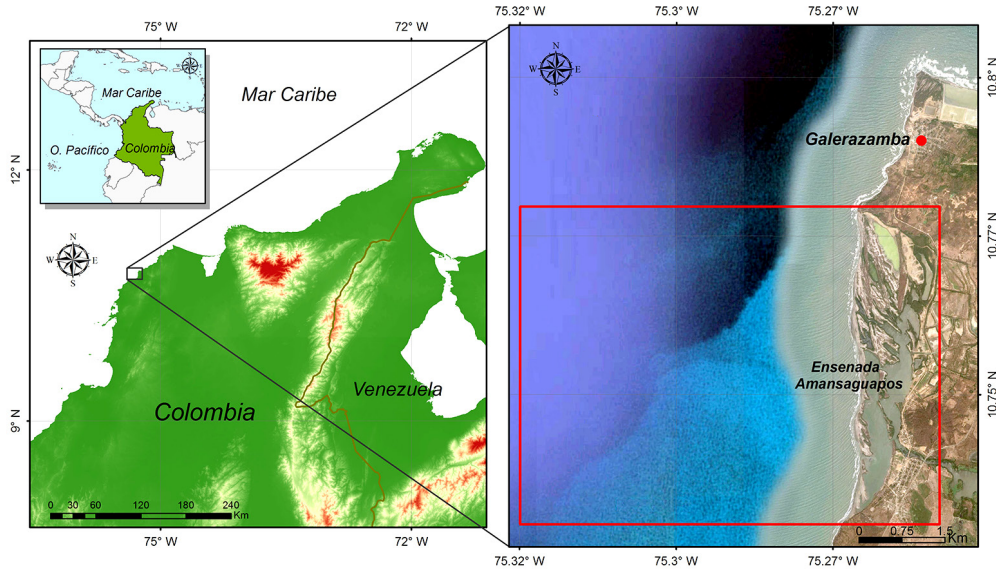


Figure 1. Study area.

Numeric scheme

Equations: Cartesian coordinates

As already mentioned, in this investigation, the mild slope equations MSE, in Cartesian coordinates, were used and given by Copeland (1985):

$$\frac{C_g}{C} \frac{\partial \eta}{\partial t} + \frac{\partial P}{\partial x} + \frac{\partial Q}{\partial y} = 0, \quad (1a)$$

$$\frac{\partial P}{\partial t} + CC_g \frac{\partial \eta}{\partial x} = 0, \quad (1b)$$

$$\frac{\partial Q}{\partial t} + CC_g \frac{\partial \eta}{\partial y} = 0, \quad (1c)$$

where η is the elevation of the free surface with respect to the average level, C and C_g are the wave velocity and the group velocity respectively, and P and Q are the vertical integration of the horizontal velocity of the particles in the x and y directions respectively, so the bathymetry is incorporated in the above mentioned equations.

Internal generation function

In order to avoid the problems derived from considering the waves as boundary conditions and

to enable wave generation through the energy spectrum, the derivation of an internal generation function is presented. Following the work of Tong Shen, Tang and Cui (2010), the inclusion of the source function in the continuity equation was considered in such a way that, being s the source term, it can be written:

$$\frac{C_g}{C} \frac{\partial \eta}{\partial t} + \frac{\partial P}{\partial x} + \frac{\partial Q}{\partial y} = s, \quad (2a)$$

$$\frac{\partial P}{\partial t} + CC_g \frac{\partial \eta}{\partial x} = 0, \quad (2b)$$

$$\frac{\partial Q}{\partial t} + CC_g \frac{\partial \eta}{\partial y} = 0, \quad (2c)$$

The solution of the previous equations, in its homogeneous version, can be written as:

$$\eta = \eta_0 \exp(i(k_x x + k_y y - \omega t)), \quad (3a)$$

$$p = p_0 \exp(i(k_x x + k_y y - \omega t)), \quad (3b)$$

$$q = q_0 \exp(i(k_x x + k_y y - \omega t)), \quad (3c)$$

being $i \equiv \sqrt{-1}$ being the imaginary constant and where $k^2 = k_x^2 + k_y^2$ must satisfy the dispersion relation, that is :

$$k^2 = \frac{\omega^2}{C^2}$$

Furthermore, p_0 y q_0 must comply:

$$p_0 = \frac{CC_g K_x \eta_0}{\omega}, \quad q_0 = \frac{CC_g K_y \eta_0}{\omega}.$$

It is assumed that being ψ anywhere between η, p, q ó s, for the full case you can write:

$$\psi(x, y, t) = \hat{\psi}(x) \exp[i(k_y y - \omega t)],$$

with $|k| < k$ and so the equations (2) are left:

$$-i\omega C_g \hat{\eta} + C \hat{p}' + ik_y C \hat{q} = c \hat{s},$$

$$-i\omega \hat{p} + CC_g \hat{\eta}' = 0,$$

$$-i\omega \hat{q} + ik_y CC_g \hat{\eta} = 0,$$

or:

$$(k^2 - k_y^2) \hat{\eta} + \hat{\eta}'' = ik \hat{s} / C_g,$$

$$\hat{p} = -iCC_g \hat{\eta}' / \omega,$$

$$\hat{q} = k_y CC_g \hat{\eta} / \omega,$$

We proceed to the solution of the equation:

$$(k^2 - k_y^2) \hat{\eta} + \hat{\eta}'' = ik \hat{s} / C_g.$$

$G_\eta(x, \varrho)$ is considered the solution for a pulse in $x = \varrho$, i. e., solution of:

$$(k^2 - k_y^2) \hat{\eta} + \hat{\eta}'' = \delta(x - \varrho).$$

To satisfy the equation automatically at all points except in $x = \varrho$,

$$G_\eta = \begin{cases} a_\eta \exp(ik_x(x - \varrho)), & \text{si } x > \varrho; \\ a_\eta \exp(ik_x(\varrho - x)), & \text{si } x < \varrho; \end{cases} \quad (4)$$

given that $k_x^2 = k^2 - k_y^2$ or that $k_x = \sqrt{k^2 - k_y^2}$. The missing point is $x = \varrho$. Integrated in x for ϱ^- a ϱ^+ :

$$k^2 - k_y^2 \int_{\varrho^-}^{\varrho^+} G_\eta dx + G'_\eta \Big|_{\varrho^-}^{\varrho^+} = 1.$$

Automatically $\int_{\varrho^-}^{\varrho^+} G_\eta dx = 0$, and therefore it must be imposed $G'_\eta \Big|_{\varrho^-}^{\varrho^+} = 1$, i. e., $2ik_x a_\eta = 1$. Now:

$$\hat{\eta}(x) = \frac{ik}{C_g} \int_{-\infty}^{+\infty} G_\phi(x, \varrho) \hat{s}(\varrho) d\varrho \quad (5)$$

and it is considered that:

$$\hat{s}(\varrho) = D \exp(-\beta \varrho^2), \quad (6)$$

Where D must be determined and $\beta = 15k_x^2$. Substituting and operating, for $x \rightarrow +\infty$, gives:

$$\lim_{x \rightarrow +\infty} \hat{\eta}(x) = \frac{ik}{C_g} D I a_\eta \exp(ik_x x), \quad (7)$$

Where $I \equiv \sqrt{\pi/\beta} \exp(-k_x^2/4\beta)$. Since you want $\eta_0 \exp(ik_x x)$ en $x \rightarrow +\infty$, it is reached:

$$D = \frac{C_g \eta_0}{ik I a_\eta} = \frac{2k_x C_g \eta_0}{k I}, \quad (8)$$

And the source function is:

$$s(x, y, t) = D \exp(-\beta x^2) \sin(k_y y - \omega t) \quad (9)$$

This ensures that at a certain distance from the source, the generated waves will possess the required characteristics of wave height and frequency.

Boundary conditions

In this model, two different contour conditions were implemented:

- Absorber frontier: The details for the implementation of the absorber frontier are explained below.
- Completely reflexive border: The implementation of this type of border has implications on the derivation matrices (see spatial discretization section) since it is imposed:

$$\frac{\partial \eta}{\partial \xi \perp} = 0, \quad P \perp = 0 \quad (10)$$

Where $\xi \perp$ is the direction perpendicular to the boundary and P is the flow in the perpendicular direction.

Numeric scheme

If you consider $x = \{x, y\}$, the equations (2) they can be rewritten as:

$$Y_0(\eta_t) = E_0(\mathbf{p}) + s(t, x) \quad (11a)$$

$$P_0(\mathbf{p}_t) = F_0(\eta) + \mathbf{d}(\eta, \mathbf{p}) \quad (11b)$$

Where $\mathbf{p} = \{P, Q\}$ and \mathbf{d} is an artificial term for the absorption of outgoing waves of the domain. This additional term, following the work of Israeli and Orszag (1981), has the form:

$$\mathbf{d} = -\omega_1 \mathbf{p} + \omega_2 \nabla \nabla \cdot \mathbf{p} + \omega_3 \sqrt{\frac{g}{h}} \eta. \quad (12)$$

The functions ω_i are space-dependent and for example, in the case of waves propagating in the positive x direction, for a buffer layer between x_a and x_b they are given by $\omega_1 = c_i \omega f(x)$, with

c a constant to be determined, ω the dominant frequency and

$$f(x) = \frac{\exp[(x - x_a)/(x_b - x_a)]^2 - 1}{\exp(1) - 1}$$

In the work of Galán *et al.* (2012) satisfactory results were obtained for values of $c_i = 7,5$ y $c_2 = c_3 = 0$, so they were taken as initial values.

Spatial discretization: matrix notation

Following the method of the lines, equations (10) are initially discretized in space. If we consider a uniform mesh of n nodal points defined by their coordinates x and y , and considering the column vectors η , P y Q , containing the n values of the variables in question, we can write the solution vector, \mathbf{f} , as:

$$\mathbf{f} = \begin{pmatrix} \eta \\ P \\ Q \end{pmatrix}.$$

In addition, you can consider the derivation matrices \mathbf{D}_x y \mathbf{D}_y in the direction x and y respectively (dimension $n \times n$) in such a way that, for example, you can write:

$$\frac{\partial \eta}{\partial x} = \mathbf{D}_x \eta.$$

Note that the construction of the derivation matrices will depend on the degree of approximation considered. With this the operator's gradient (\mathbf{gr}) and divergence (\mathbf{dv}) are given by:

$$\mathbf{gr} = \begin{pmatrix} \mathbf{D}_x \\ \mathbf{D}_y \end{pmatrix}, \quad \mathbf{dv} = (\mathbf{D}_x \ \mathbf{D}_y).$$

Using this notation, equations (11) can be written as:

$$\mathbf{L} \cdot \mathbf{f}_t = \mathbf{R} \cdot \mathbf{f} + X(t, \eta, \mathbf{p}). \quad (13)$$

The matrices \mathbf{L} and \mathbf{R} are:

$$\mathbf{L} = \begin{pmatrix} \mathbf{L}_{11} & \mathbf{0}_{n \times 2n} \\ \mathbf{0}_{2n \times n} & \mathbf{L}_{22} \end{pmatrix}, \mathbf{R} = \begin{pmatrix} \mathbf{0}_{n \times n} & \mathbf{R}_{12} \\ \mathbf{R}_{21} & \mathbf{0}_{2n \times 2n} \end{pmatrix}, \quad (14)$$

With:

$$\mathbf{L}_{11} = \overline{C_g/C}, \quad (15a)$$

$$\mathbf{L}_{22} = \mathbf{I}_{2n}, \quad (15b)$$

$$\mathbf{R}_{12} = -d\mathbf{v}, \quad (15c)$$

$$\mathbf{R}_{21} = -\overline{CC_g} \mathbf{g}\mathbf{r}. \quad (15d)$$

For more information about the construction of the matrices involved, consult Galán *et al.*, (2012).

Temporary integration: explicit scheme Runge-Kutta of 4th order

Equation 15 is a linear system of partial differential equations for the nodal values of the unknowns. This system can be rewritten as:

$$\mathbf{f}_t = \mathbf{L}^{-1} \cdot \mathbf{r}(t, \mathbf{f}), \quad (16)$$

Where $\mathbf{r} = \mathbf{R} \cdot \mathbf{f} + X(t, \eta, \mathbf{p})$. For reasons of stability discussed below, an explicit fourth-order Runge-Kutta scheme (RK4) is chosen for the temporal integration, being \mathbf{f}^n the solution at the time $\mathbf{t}_n = \mathbf{t}_0 + n\Delta t$ you can write:

$$\mathbf{f}^{n+1} = \mathbf{f}^n + \Delta t \frac{\mathbf{K}_1 + 2\mathbf{K}_2 + 2\mathbf{K}_3 + \mathbf{K}_4}{6}, \quad (17)$$

Where:

$$\mathbf{K}_1 = \mathbf{L}^{-1} \cdot \mathbf{r}(t^n, \mathbf{f}^n), \quad (18a)$$

$$\mathbf{K}_2 = \mathbf{L}^{-1} \cdot \mathbf{r}(t^n + \Delta t/2, \mathbf{f}^n + \Delta t\mathbf{K}_1/2), \quad (18b)$$

$$\mathbf{K}_3 = \mathbf{L}^{-1} \cdot \mathbf{r}(t^n + \Delta t/2, \mathbf{f}^n + \Delta t\mathbf{K}_2/2), \quad (18c)$$

$$\mathbf{K}_4 = \mathbf{L}^{-1} \cdot \mathbf{r}(t^n + \Delta t, \mathbf{f}^n + \Delta t\mathbf{K}_3). \quad (18d)$$

Therefore, in each step of time it is necessary to solve 4 systems of equations where the matrices of the system are diagonal and dispersed.

Linear stability

If the source terms and amortization terms in expression (16) are eliminated, we have:

$$\mathbf{f}_t = \mathbf{A} \cdot \mathbf{f} = (\mathbf{L}^{-1} \cdot \mathbf{R}) \cdot \mathbf{f}, \quad (19)$$

For the numerical model to be stable, it must be imposed that all the eigenvalues of the matrix \mathbf{A} , v_j , multiplied by the temporal step Δt , represented in the real-imaginary plane, are found within the stability region of the method of chosen integration. Figure 2 shows the stability region for the 3rd order Adams-Bashford scheme (AB3), for the 4th order Adams-Moulton scheme (AM4) and for the 4th order Runge-Kutta scheme (RK4). As can be seen, the region of stability of greater extension corresponds to the method of 4th order, which is why it has been chosen for the present work as a method of temporal integration allowing greater values of the temporal passage, and therefore, a higher computation speed.

From Figure 2 it can be seen that, by defining $v_{\max} = \max |v_j|$, the RK4 method provides stable schemes for:

$$v_{\max} \Delta t \lesssim 2,8278, \quad (20)$$

This can be considered as a CFL condition necessary for stability. In one dimension, in the case of a flat bottom, the value of v_{\max} depends on ω , g , h and Δx ; in addition to the order of the approximation used for the computation of the spatial derivatives, o , and also the number of nodes, n . By dimensional analysis:

$$\frac{v_{\max} \Delta x}{\sqrt{gh}} = f_x \left(\pi_1 \equiv \frac{\Delta x}{h}, \pi_2 \equiv \frac{\omega^2 h}{g}, o, n \right). \quad (21)$$

Figures 3 and 4 show the behavior of the function f_x for different values of π_1 and π_2 . In both cases, $n = 5$ has been taken, given that the influence of n has been proven to vanish for values of $n \geq 20$.

As can be seen, the stability function f_x is independent of the group value π_1 . Also, for high values of the group π_2 , the function tends to zero; while for small values, it becomes constant with limits:

$$\lim_{\pi_2 \rightarrow -\infty} f_x = \begin{cases} 1,0000, & 2^\circ \text{ orden en espacio} \\ 1,3722, & 4^\circ \text{ orden en espacio} \end{cases} \quad (22)$$

According to expressions (19) and (20), the temporary step should be chosen so that:

$$\frac{\sqrt{gh\Delta t}}{\Delta x} \lesssim \frac{2,8278}{f_x}, \quad (23)$$

Or what is the same, in 1D, the Courant-Friedrich-Levy (CFL) condition remains as:

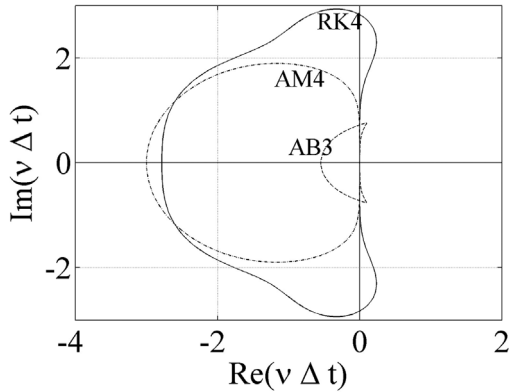


Figure 2. Stability regions for the 3rd order Adams-Basforth scheme (AB3), for the 4th order Adams-Moulton scheme (AM4) and for the 4th order Runge-Kutta scheme (RK4).

$$\frac{\sqrt{gh\Delta t}}{\Delta x} \lesssim \begin{cases} 2,828, & 2^\circ \text{ orden en espacio,} \\ 2,061, & 4^\circ \text{ orden en espacio.} \end{cases} \quad (24)$$

In the 2D case, the stability analysis is similar, starting from the dimensional analysis (for n large enough) we have:

$$\begin{aligned} & \frac{v_{\max} \Delta s}{\sqrt{gh}} \\ &= f_s \left(\pi_1 \equiv \frac{\Delta s}{h}, \pi_2 \equiv \frac{\omega^2 h}{g}, \pi_3 \right. \\ & \left. \equiv \frac{\Delta x}{\Delta y}, 0 \right), \end{aligned} \quad (25)$$

With $\Delta s^2 = \Delta x^2 + \Delta y^2$. taking $\Delta x = \Delta y$ the function f_s presents as limits:

$$\lim_{\pi_2 \rightarrow -\infty} f_s = \begin{cases} 2,0000, & 2^\circ \text{ orden en espacio,} \\ 2,7444, & 4^\circ \text{ orden en espacio,} \end{cases} \quad (26)$$

Obtaining as a condition CFL in 2D:

$$\frac{\sqrt{gh\Delta t}}{\Delta s} \lesssim \begin{cases} 1,414, & 2^\circ \text{ orden en espacio,} \\ 1,030, & 4^\circ \text{ orden en espacio.} \end{cases} \quad (27)$$

For values of $Dx \neq Dy$ a similar stability analysis can be carried out, obtaining different CFL conditions.

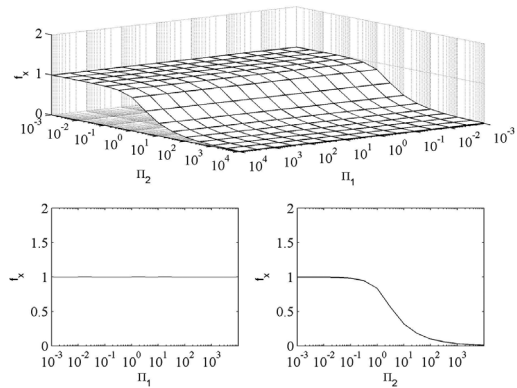


Figure 3. Behavior of the function f_x for derivatives of order 2. It has been taken $n = 50$ since it is observed that f_x stops depending on n for values above 20.

Sediment transport

Modification of breaking waves

The hydrodynamic module propagates wave trains from deep water to shallow water. Although the model solves the linear equations under the mild slope hypothesis, when the camber of the wave is sufficiently high, the wave undergoes a rupture process, dissipating energy and increasing the solid flow in the surf zone.

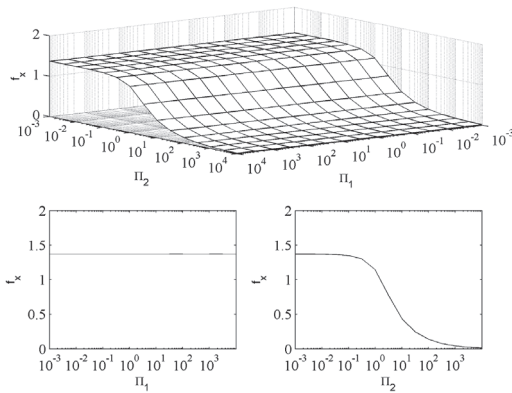


Figure 4. Behavior of the function f_x for derivatives of order 4. It has been taken $n = 50$ since it is observed that f_x stops depending on n for values above 20.

To simulate numerically this process, an artificial dissipation of energy has been added, so that a "sponge layer" is applied, through the variable $C_{s,rotura}$, internal to the domain, whose value will be given by:

$$C_{s,1} = \begin{cases} 1 & \text{si } \frac{|\eta|}{h} \leq \epsilon \\ \left(\frac{|\eta|}{h} - \epsilon\right)^{0.5} & \text{si } \frac{|\eta|}{h} > \epsilon \end{cases}, \quad C_{s,rotura} = \min\{C_{s,1}, 2\},$$

Where ϵ is a parameter to calibrate. For the previous numerical results a value of $\epsilon \approx 0.3$ has been taken.

Expressions used to obtain the speed in the background

From the simulation carried out with the hydrodynamic module, the free surface, η and the variables P and Q are obtained for each point,

as shown in Figure 5. Since wave generation is carried out for multi-chromatic wave trains, it is required that the exit time of the model is a multiple of the wave periods considered. For the example considered, since a bi-chromatic wave is being generated, with periods $T = 5s$ y $T = 7s$, the data output will have at least a duration of $t_{max} = 35s$.

From the time series of the variables P and Q, the unit vector that defines the direction of the wave vector can be obtained,

$$\mathbf{k} = |\mathbf{k}| \mathbf{e}_k = \sqrt{k_x^2 + k_y^2} \mathbf{e}_k$$

$$\mathbf{e}_k = \{\cos\phi, \sin\phi\}, \quad \phi = \arctan \frac{Q}{P}$$

According to Airy's theory, for a progressive wave ($x = \{x, y\}$), the free surface is:

$$\eta = \eta_0 \cos(\mathbf{k} \cdot \mathbf{x} - \omega t),$$

Being η_0 the wave amplitude and $\omega = 2\pi/T$ the frequency. In the case of a wave train, the surface will be given by:

$$\eta = \sum_i \eta_{0,i} \cos(\mathbf{k}_i \cdot \mathbf{x} - \omega_i t),$$

Where the sub-indices "i" indicates the i^{th} component of the generated wave train. Likewise, the horizontal velocity, $\mathbf{u} = \{u, v\}$ for a monochromatic wave will be given by:

$$\mathbf{u}(z) = \eta_0 \omega \frac{\cosh[\mathbf{k}(h+z)]}{\sinh(\mathbf{k}h)} \cos(\mathbf{k} \cdot \mathbf{x} - \omega t),$$

Where h is the depth at which the wave propagates. From the above, the velocity in the background $z = -h$ will be:

$$\mathbf{u}_b = \eta_0 \omega \frac{\cos \mathbf{k} \cdot \mathbf{x} - \omega t}{\sinh(\mathbf{k}h)}$$

That is to say:

$$\mathbf{u}_b = \eta\omega / \sinh(\mathbf{k}h),$$

However, for shallow waters, where the transport of sediments is more significant $\sinh(\mathbf{k}h) \rightarrow kh$, and therefore:

$$\mathbf{u}_b = \frac{\eta\omega}{\mathbf{k}h} = \frac{\eta\mathbf{C}}{h}$$

Where C is the speed of the wave. In this way, the velocity history for the same point shown in the Figure 5 is shown in the Figure 6.

It can be shown that, as it is a linear wave propagation model, the temporal averages of the velocities are zero, and therefore, sediment transport will also be zero. Hence, a modification in the series of speeds must be introduced according to the Stokes theory. For a progressive (linear) monochromatic wave, defined by its free surface and speed as:

$$\eta = \eta_0 \cos(\mathbf{k}\mathbf{x} - \omega t),$$

$$U_b = U_{b,0} \cos(\mathbf{k}\mathbf{x} - \omega t),$$

$$V_b = V_{b,0} \cos(\mathbf{k}\mathbf{x} - \omega t),$$

It can be verified that, according to the Stokes theory, the speed under the crest and under the trough of the wave will be given by:

$$U_{b,cresta} = U_{b,0}\alpha, \quad V_{b,cresta} = V_{b,0}\alpha,$$

$$U_{b,seno} = (2 - \alpha)U_{b,0}, \quad V_{b,seno} = (2 - \alpha)V_{b,0},$$

Donde:

$$\alpha = 1 + 0.3 \frac{H_s}{h}$$

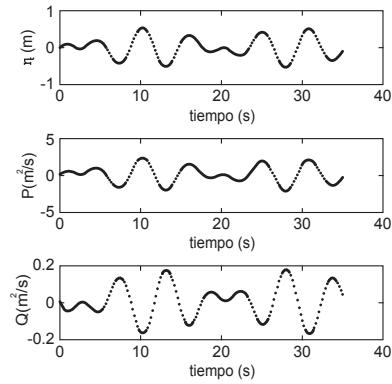


Figure 5. Example of time series for introduced waves of $T = 5s$ y $T = 7s$

In the previous expression, H_s is the significant wave height. In this way, from a linear (symmetric) wave, a non-linear wave can be assimilated, with non-zero sediment transport. Thus, for each point the procedure followed will be:

1. Get the time series of velocity in the background for the propagated wave
2. Find H_s for each point and with it the value of α
3. For each point, obtain η_0 , $U_{b,0}$ y $V_{b,0}$ as the mean value of the amplitude of the speed for the different propagated waves
4. Assimilate the propagated wave to a monochromatic wave of amplitudes for free surface and velocity η_0 , $U_{b,0}$ y $V_{b,0}$ in crest and trough

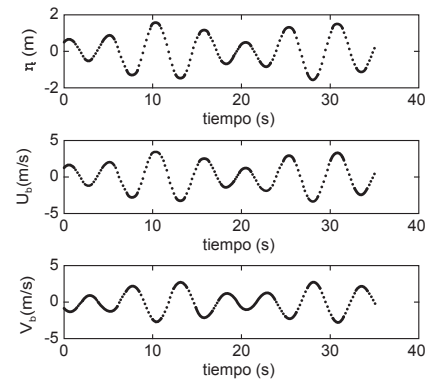


Figure 6. Example of time series of velocities in the background for introduced waves of $T = 5s$ y $T = 7s$.

Expressions used to obtain sediment tension and transport

The tangential stress transmitted to the background can be expressed as:

$$\tau_b = \frac{1}{2} \rho f_w U_\delta^2,$$

Where ρ is the density of the fluid, f_w is the coefficient of friction and U_δ is the instantaneous velocity near the bottom. For rough turbulent flow, in Johnson (1996), the coefficient of friction was expressed as:

$$f_w = \exp \left[-6 + 5.2 \left(\frac{A_b}{k_{sw}} \right)^{-0.19} \right],$$

Where A_b is the wave amplitude at the bottom and k_{sw} the equivalent roughness, which can usually be taken as $k_{sw} \approx 2d_{50}$ where d_{50} is the average sediment size. For the previous expression:

$$A_b = \frac{H/2}{\sinh(2kh)},$$

Where $H = 2\eta_0$ is the height of the waves. For the calculation of solid transport the formulation of Van Rijn and Kroon (1992) will be used, where the solid flow of instantaneous background in m^2 / s will be given by

$$\frac{q_b(t)}{d_{50} d_{50,*}^{-0.3} u_*} = 0.25 \alpha_b \left(\frac{\tau_b - \tau_c}{\tau_c} \right)^{3/2},$$

Since τ_c is the critical tension at the beginning of the movement, obtained by means of the Shields parameter, and:

$$u_* = \sqrt{\frac{\tau_b}{\rho}}, \quad \alpha_b = 1 - \left(\frac{H_s}{h} \right)^{\frac{1}{2}}, \quad d_{50,*} = \left(\frac{g \Delta d_{50}^3}{v^2} \right)^{\frac{1}{3}},$$

With v the dynamic viscosity of the fluid and $\Delta = (\rho_s - \rho) / \rho$ the submerged relative density. The critical tension of the beginning of the movement can be found using the abacus of Shields (1936), for example:

$$\frac{\tau_c}{\rho g \Delta d_{50}} = \frac{0.23}{d_{50,*}} + 0.054 \left[1 - \exp \left(-\frac{d_{50,*}^{0.85}}{23} \right) \right].$$

Modification of the bathymetry

For the modification of the bathymetry it is assumed that sediment transport was maintained during the considered sea state, so that once the value of $q_b(t)$, the average value in each point in vector form is found, that is to say:

$$\overline{\mathbf{q}_b} = \left(\frac{1}{t_{max}} \int_{t=0}^{t=t_{max}} q_b(t) dt \right) \mathbf{e}_k.$$

For the modification of the bathymetry the formulation of Exner is used, where:

$$\frac{\partial h}{\partial t} = -\frac{1}{1-n} \nabla \cdot \overline{\mathbf{q}_b},$$

So, considering Euler's method for temporal integration, we obtain:

$$h^{n+1} = h^n + \Delta t \frac{\partial h}{\partial t},$$

Numerical examples:

1D source function and absorbent conditions

In this numerical example we try to show the accuracy of the generation of the source function in 1D. To do this, a monochromatic wave train on a flat background is generated and compared with the Airy solution (linear wave theory). For the example, we have taken a wave period $T = 0,5s$ and an acceleration of gravity $g = 9,8m/s^2$ propagating over a depth of $h = \{1, 10, 25, 50\}$. The linear theory of Airy yields values of wavelength and celerity collected in table 1. It is desired that the wave to be generated has an amplitude of $\eta_0 = 1m$. The stability condition for all

cases would be in $CFL = 0,9$ con $\sigma = 4$ y $n = 1000$ y $dx = 0,25m$.

Figure 7 shows the amplitudes obtained at the different depths compared to the amplitude required for a time $t = 10T$, sufficient for the wave to reach the contour. In all cases, the wave generated has the required amplitude, and the generation in case 1D is validated. In the same way it is verified that the absorption function also works properly in both frontiers (the generation takes place in the center of the domain and both borders are absorbent).

Table 1. Values of wavelength and celerity calculated with the Airy term. The period $T = 0,5s$ and the gravity $g = 9,8m/s^2$ remain constant.

$h(m)$	$\lambda_{Airy} (m)$	$C_{Airy} (m/s)$
5	30.323	6.064
10	36.614	7.322
25	39.035	7.807
50	39.060	7.812

2D source function and absorbent conditions

To verify the proper functioning of the source function in the 2D case, the same example as in generation 1D (previous section) will be taken, considering only the case where $h = 5$ m. The angle of incidence is 30° and the length in front is 50m.

As in the case 1D, the amplitude of the wave is the required. In addition, the angle of incidence coincides exactly with that imposed, thus validating the function of internal generation of waves in 1D and 2D. The absorbent boundary conditions do not introduce instabilities or fictitious waves in the study domain (Figure 8).

Case study: Cone shaped emerged island and reflective conditions

For the study of the introduction of the coastline and the treatment of these borders, the bathymetry of the experiment by Briggs, Synolakis, Harkins and Green (1995) has been implemented. It is a cone shaped island emerged in a tank of 25 m long and 30m wide and a depth of 0.32 m. The island is centered at the

point $x_c = 13m$ e $y_c = 15m$ and has a base diameter of 7.2m. At the level of the free surface the diameter is 4.64m and in the upper part it is 2.2 m (the inclination of the slopes of the island is 1: 4). The boundary conditions have been considered as purely reflexive and as an initial condition a solitary wave is introduced (test 3 in Briggs *et al.*, 1995) of the form:

$$\eta(x, t = 0) = H \operatorname{sech}^2 [\gamma(x - x_c)], \tag{28}$$

With $\gamma = \sqrt{0,75H}$ y x_c and x_c being the center of the solitary wave. In the case considered $H = 0,20m$. Figures 9 and 10 show the free surface at different moments of time. As can be seen, both the purely reflexive conditions and the treatment of the internal islands and coastlines are working correctly, not generating instabilities in the model.

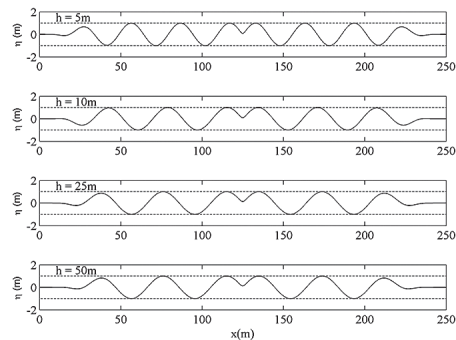


Figure 7. Generation of 1D monochromatic wave with 1D con $T = 5s$ y $g = 9,8m/s^2$ on a flat bottom of different depth. Values obtained for a time $t = 10T$.

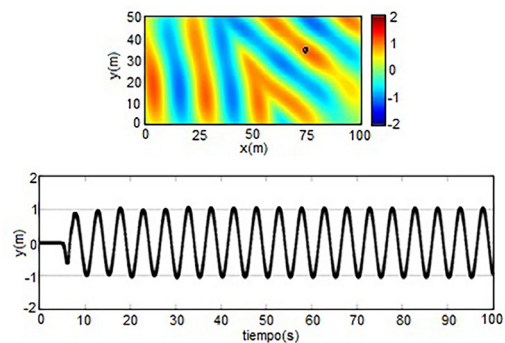


Figure 8. 2D monochromatic wave generation with $T = 5s$ y $g = 9,8m/s^2$ on a flat bottom of depth $h = 5m$ with angle of incidence $\phi = 30^\circ$. Top screenshot for time $t = 10s$ y and target point marked with black circle. Below temporary elevation series detected at target point.

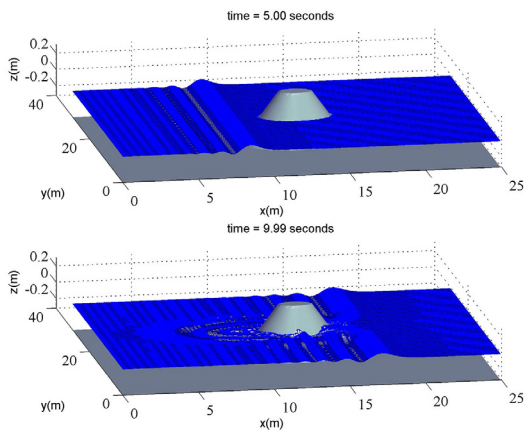


Figure 9. Case example: cone shaped island (1/2).

Table 2. Characteristics of the mesh used in the simulation for the Galerazamba area.

Characteristics	Detail
Number of mesh points in the direction of wave advance	1546
Number of mesh points in a direction perpendicular to the wave advance	437
Mesh resolution in the direction of wave advance	1 m
Resolution of mesh in direction perpendicular to the wave advance	3 m
Wave incidence angle	N 90' E

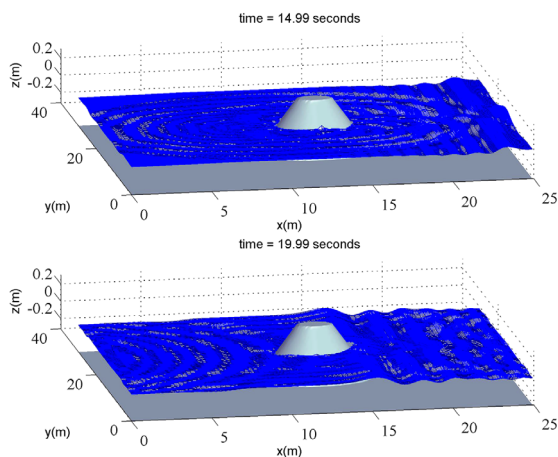


Figure 10. Case example: cone shaped island (2/2).

RESULTS

Previous Results

To check the correct functioning of the model, a calculation grid was generated in the Galerazamba area, whose characteristics are shown in Table 2.

The introduced wave is a bi-chromatic wave train with periods of 8 and 10s respectively and wave heights of 0.8 m for both components (expected maximum wave heights of 1.6m). The sea state is considered with a duration of 3 hours. The Figure 11 shows the initial bathymetry of the study area. Wave generation occurs in deep water, more specifically at $x = 300\text{m}$.

The Figure 12 shows the hydrodynamic variables obtained with the propagation module for a point located near the zone of rupture. It should be noted that the magnitude of the variable P, which measures the "mass transport" in the "x" direction, is one order of magnitude greater than the magnitude Q that measures transport in the perpendicular direction, as expected. The mean solid flow rate along the sea state can be seen in Figure 13. Associated with this flow rate, the variation of the bottom along the 3 hours of sea state is shown in Figure 14. to be appreciated, there is a clear predominance of solid transport in a first zone of rupture, after which, the loss of wave energy decreases the intensity of this transport.

Thus, the modified bathymetry by the state of the sea is represented in the Figure 15.

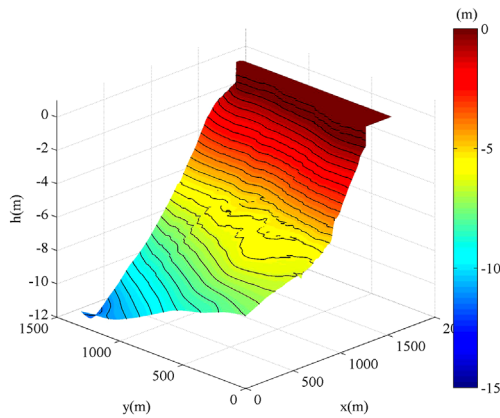


Figure 11. Initial bathymetry in the study area.

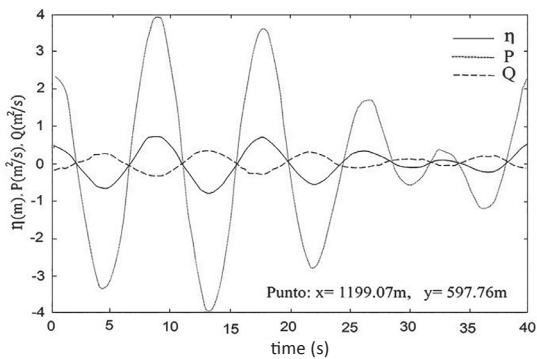


Figure 12. Time series of the free surface $\eta(t)$ and of the variables P and Q for a point located near the rupture zone.

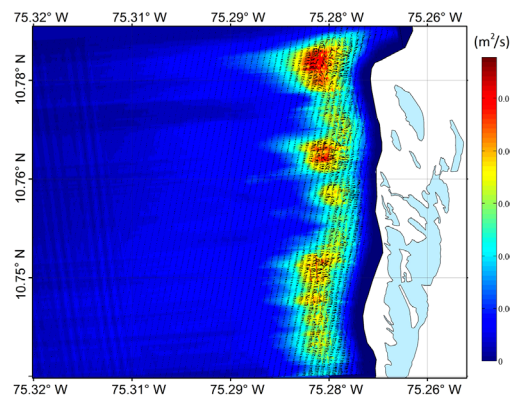


Figure 13. Average solid flow during sea state in m^2 / s in module (colors) and direction (arrows).

DISCUSSION

The models that solve the phase, such as those based on the MSE, have an advantage over the spectral models, as there is no loss of information from the phase, because the height of the sheet is obtained in a deterministic way at every moment and in every point.

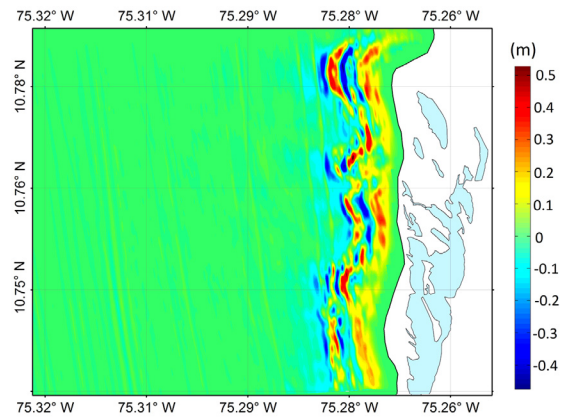


Figure 14. Variation in the bathymetry during the sea state. Negative values in the variation of the seabed indicate erosion, positive values show deposition of sediments.

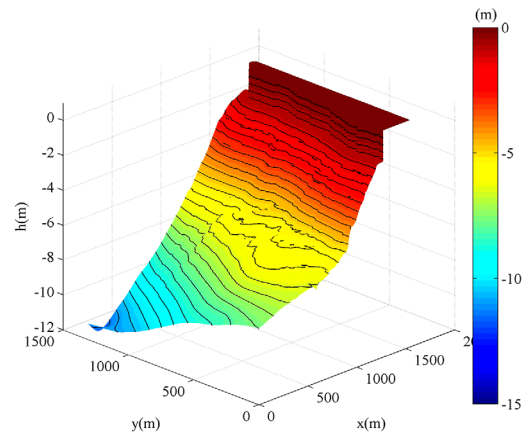


Figure 15. Final bathymetry after the propagation and the computation of sediment transport.

In spite of this, the implementation of this type of models is limited due to the high computational cost required, taking into account that the mesh sizes must be of the order of $L / 50$ or $L / 20$;

where L is the wavelength characteristic of the swell; and the passage of time for the temporary integration one or two orders of magnitude lower than the characteristic period of the swell (Universidad de la Coruña, 2013).

So that, based on the hyperbolic form of the smooth slope equation, the model developed in the present investigation, implements the fourth order Runge-Kutta scheme (RK4) as a temporary integration method, allowing greater values of the temporary step, and therefore, a higher computation speed, with which the aforementioned drawback is partially solved.

The elliptical form of the MSE equation implies the imposition of boundary conditions on all domain boundaries in the models that use it (eg MSP-IH Cantabria and MIKE 21 EMS-DHI), generating problems regarding the conditions of absorption for oblique incidence of the waves due to the appearance of unwanted reflections, from the numerical modeling. In addition, for propagation on very large surfaces, the finite element method requires the use of large meshes, which translates into a high computation time (Losada, I.J., Medina, Losada, M.A & Vidal, 1995). Other models have developed a parabolic extension of this equation, which allows to apply boundary conditions (reflective or open) only in the swell incidence contours, assuming that the wave propagates in a predominant direction (eg OLUCA-IH Cantabria, MIKE 21 PMS-DHI), which is a disadvantage compared to the hyperbolic models, since, in the case of waves changing direction, the calculation mesh should also be modified to align with it. Compared with elliptical models, hyperbolic models offer the advantage of the reduction in calculation time, particularly in two-dimensional domains and, in addition, they are capable of incorporating arbitrary intensity contours for reflection, refraction and diffraction mechanisms (Lee *et al.*, 1998). In this sense, the absorbent and reflective contour conditions applied in this investigation, proved not to generate instabilities and function correctly, as can be observed in the different tests carried out, where for the absorbing conditions, the model responds satisfactorily to the exercises in which the Airy solution was applied and the test

with the bathymetry of Briggs *et al.*, (1995) for reflective conditions, all of them with efficient computation times.

Taking into account that the model developed in this study was carried out within the framework of the LIZC project, a sediment transport module was implemented as a complementary part, which is responsible for solving the transport of sediments and the morphological evolution of the coastal bathymetry, from the results of the hydrodynamic module. Since the transport of sediments depends on the circulatory system in the surf zone, which in turn is induced by waves (Losada *et al.*, 1995), it is necessary to consider that the hydrodynamic equations used here solve a linear model, and for this it was necessary to adapt the data in such a way that the transformation of a completely linear swell (without transport of sediments) into a non-linear swell was made. Numerous authors have developed modifications and extensions to the equation of the mild slope using the theories of Airy, Stokes, and in the expression of Hedges among others, with the purpose of solving the wave-current interaction. The equation developed in this research makes use of the Stokes theory to modify the speed under the crests and the troughs of a wave, by assimilating a non-linear wave with non-zero sediment transport, which demonstrated the expected performance as can be seen in the Figure 6.

In this order of ideas, the sediment transport module, executed once the hydrodynamic module results were obtained for the exercise in Galerazamba, showed the good performance of the formulations applied (Figures 12 - 14), beginning with the proposal by Van Rijn and Kroon (1992), for solid transport. This proposal is one of the most used at present in coastal environments to provide a low dispersion with respect to measurements (Cinat, 2012), and whose effectiveness was proven by Bayram, Larson and Hanson (2007), for tidal currents and in the surf zone. Similarly, the Exner equation, used to describe the evolution of the background after simulating a sea state, also proved fulfil its objective.

CONCLUSIONS

A model based on the "mild-slope" equations was developed with the capacity to feed the LIZC model, showing a high computational performance, for which an internal generation function was configured and validated in the cases 1D and 2D; verifying that the created waves possess the required amplitudes, and the incidence angle exactly matches that imposed. In addition, it was verified that the reflective and absorbent conditions applied did not generate instabilities or fictitious waves. Regarding the case applied in the Galerazamba area, the model presented a coherent response with respect to the formulations applied for the transport of sediments and the modification of the seabed.

BIBLIOGRAPHIC REFERENCES

- Bayram A., Larson M., Hanson H. (2007). A new formula for the total longshore sediment transport rate. *Coastal Engineering*, 54:700–710.
- Berkhoff, J. C. W. (1972). "Computation of Combined Refraction-Diffraction." *Proceeding of the 13th International Conference Coastal Engineering*, Vancouver, ASCE, 1, 471-490.
- Bokaris, J., Anastasiou, K. (2003). Solution of the hyperbolic mild-slope equations using the finite volume method. *International Journal for numerical methods in fluids*. Volume 41, 225-250.
- Briggs, M. J., Synolakis, C. E., Harkins, G. S., Green, D. R. (1995). Laboratory experiments of tsunami runup on a circular island, *PA-GEOPH 144 (3/4)*, 569-593.
- Cinat, P. (2012). Sediment transport models for shallow waters equations. (Tesis Maestría). Universidad de Pisa. Pisa, Italia.
- Recuperado de: https://project.inria.fr/mediagoon/files/2012/11/TesiSWE_Cinat.pdf.
- Copeland, G. J. M. (1985) "A Practical Alternative to the "Mild Slope" Wave Equation." *Coastal Engineering*, Vancouver, 9(2), 125-149.
- Galán, A., Simarro, G., Orfila, A., Simarro, J. Liu, P. L.-F. (2012). "A fully nonlinear model for water wave propagation from deep to shallow waters". *Journal of Waterway, Port, Coastal and Ocean Engineering-ASCE*, 138:5, 362-371.
- Israeli, M., y Orszag, S. (1981). "Approximation of radiation Boundary conditions". *J. Comp. Phys.* Vol 41, 115-135.
- Jonsson, I. G. (1966). Wave boundary layers and friction factors, in *Proceedings of 10th Conference on Coastal Engineering*, pp. 127–148, Am. Soc. of Civ. Eng., Reston, Va.
- Lee, C., Park, W.S., Cho, Y-S., y Suh, K.D. (1998). Hyperbolic mild-slope equations extended to account for rapidly varying topography. *Coastal Engineering*, Volumen 24, 243-257.
- Losada, I.J., Medina, R., Losada, M.A., Vidal, C. (1995). Modelos hidrodinámicos y de transporte de sedimentos. *Ingeniería del agua*, [S.l.], v. 2, n. 1, mar. ISSN 1886-4996.
- Shields, A. (1936). "Anwendung der Ähnlichkeitsmechanik und der Turbulenzforschung auf die Geschiebebewegung, "[Application of similarity principles and turbulence research to bedload movement]. *Mitteilungen der Preußischen Versuchsanstalt für Wasserbau und Schiffbau*, Berlin, 26, 26 pp.
- Song, Z., Zhang, H., Kong, R. Li., Zhang, W. (2007). An efficient numerical model of hyperbolic mild-slope equation. In *proceedings of the international conference on Offshore mechanics and Arctic engineering – OMAE*, vol 5, pages 253-258.
- Suh, K.D., Lee, C., Park, W.S. (1997). Time-dependent equations for wave propagation on rapidly varying topography. *Coastal Eng.* 32, 91–117.
- Tong, F.F., Shen Y., Tang J. y Cui L. (2010). Water wave simulation in curvilinear coordinates using a time-dependent mild slope equation." *Journal of Hydrodynamics*, Ser. B, 22(6), 796 - 803.
- Universidad de la Coruña- E.T.S Ingenieros de Caminos, Canales y Puertos. (2013). *Análisis*

comparativo de diferentes metodologías para el cálculo de corrientes litorales generadas por oleaje. Recuperado de: <http://www.gea-ma.org/hidraulica/index.php?s=39>

Van Rijn, L.C. y Kroon, A. (1992). Sediment transport by currents and waves. Proc. 23rd Intern. Conference on Coastal Engineering, Venice, 2613-2628.